
A Baseline Method for Removing Invisible Image Watermarks using Deep Image Prior

Hengyue Liang

*Electrical and Computer Engineering
University of Minnesota, Twin Cities*

liang656@umn.edu

Taihui Li

*Computer Science and Engineering
University of Minnesota, Twin Cities*

lixx5027@umn.edu

Ju Sun

*Computer Science and Engineering
University of Minnesota, Twin Cities*

jusun@umn.edu

Abstract

Image watermarks have been considered a promising technique to help detect AI-generated content, which can be used to protect copyright or prevent fake image abuse. In this work, we present a black-box method for removing *invisible* image watermarks, without the need of any dataset of watermarked images or any knowledge about the watermark system. Our approach is simple to implement: given a *single* watermarked image, we regress it by deep image prior (DIP). We show that from the intermediate steps of DIP one can reliably find an evasion image that can remove invisible watermarks while preserving high image quality. Due to its unique working mechanism and practical effectiveness, we advocate including DIP as a baseline invasion method for benchmarking the robustness of watermarking systems. Finally, by showing the limited ability of DIP and other existing black-box methods in evading training-based *visible* watermarks, we discuss the positive implications on the practical use of training-based *visible* watermarks to prevent misinformation abuse. Our code is publicly available at https://github.com/HengyueL/DIP_Watermark_Evasion.

1 Introduction

In this prosperous era of generative AI, the traceability of AI-generated content (e.g., language, images, and videos) to its source has been frequently mentioned as a promising solution to promote the responsible use of generative AI (Fan et al., 2023), e.g., to protect copyright or to curb misinformation. In particular, the traceability of AI-generated images has become increasingly urgent, as many AI products, such as DALL-E (Ramesh et al., 2022) and Stable Diffusion (Rombach et al., 2022), can create highly photorealistic and artistic images that are hard to distinguish from natural photos or human drawings. Unsurprisingly, some AI-generated images have caused false beliefs on social media (Wendling). Thus, major tech companies such as Google, OpenAI (Bartz & Hu) have recently opted to incorporate watermarks into their image generation products to improve traceability and promote responsible use.

Manually designed vs. training-based watermarks Watermarking methods can be generally divided into two categories: (i) *non-blind* methods (Cox et al., 1997; Hsieh et al., 2001; Pereira & Pun, 1999) and (ii) *blind* methods (Bi et al., 2007), which are divided by whether access to original clean images is required to correctly decode the watermarked images (Zhao et al., 2024). In what follows, we focus only on blind methods (and refer to them as *watermarks*), as they do not require access to clean images and fit better in large-scale application scenarios, such as tracing AI-generated content. Watermarks are typically embedded



Figure 1: Example of (a) a clean image, (b) an image with an overlaid logo watermark and (c) an image with steganography watermark.

in images in terms of an overlaid logo or steganography¹ (Morkel et al., 2005); see Fig. 1 for an example. The embedded watermarks then are typically detected by human eyes or by algorithmic decoders (Voyatzis & Pitas, 1999; Zhu et al., 2018). In early research, various manually designed watermarks were proposed and applied to copyright protection, e.g., visible watermarks (detectable by human eyes) such as an overlaid layer (Kankanhalli et al., 1999) or a color code signature (such as the example in Appendix A); invisible watermarks (detectable by algorithmic decoders) such as Tirkel et al. (1993); Pereira & Pun (2000); Navas et al. (2008). However, these manually designed watermarks are challenged by robustness concerns, i.e., imperceptible corruption, digital editing, or deliberate attacks to the watermarked image can make them undetectable (Mishra, 2022; Zhao et al., 2023); see also Fig. 2. To address these challenges, recent work has shifted to training-based watermarking systems using deep neural networks (DNNs). By incorporating ideas from data augmentation (Mumuni & Mumuni, 2022) and adversarial training (Goodfellow et al., 2014b), the robustness of training-based watermarks against common digital corruptions consistently beats that of manually designed ones (Zhu et al., 2018; Zhang et al., 2019b; Tancik et al., 2020; Jia et al., 2021).

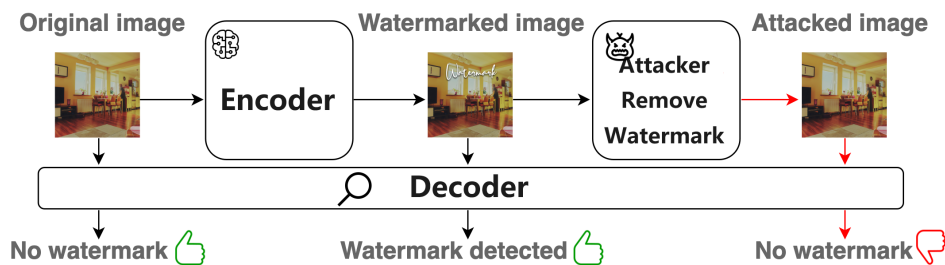


Figure 2: Illustration of the watermarking system and the robustness concern—watermarks may be removed with little loss of image quality.

Evaluating the robustness of watermark systems Robustness evaluation of watermark systems often operates under either the white-box or the black-box evasion (i.e., attack) setting (Zhao et al., 2024; An et al., 2024). In white-box evasion, the decoder and the groundtruth watermark are accessible to a dedicated evader (Jiang et al., 2023), which easily leads to a high threat. In contrast, the threat can be greatly reduced by maintaining secrecy of the system (An et al., 2024), i.e., under the *black-box* model, where the decoder and the groundtruth watermark remain unknown to the evader. Nowadays, it is common for companies not to open-source their generative products, e.g., DALLE-3 from OpenAI, Midjourney, Imagen from Google. Thus, being robust against potential black-box evasions is of higher priority in practical scenarios.

The main focus of this paper is to explore *black-box* evasion techniques that can generate evasion images with the best possible quality. We stress the image quality alongside the evasion success, because for a dedicated evader, the higher the quality of the evasion images they can produce, the more benefit they can potentially gain, e.g., breaking the copyright protection without compromising the image quality or misleading people

¹Steganography: detectable messages embedded in an image but are invisible to human eyes.

to use highly naturally-looking fake images. Recently, researchers are putting effort into standardizing the robustness benchmark of image watermarks (An et al., 2024). Although the selected black-box evasion methods are effective in bypassing watermark detection, their evasion images can still introduce visible defects; see Section 4 and Fig. 8. Thus, the search for new methods to provide stronger stress tests of watermarking systems is still a pressing problem.

Our contributions In this paper, we propose a new black-box watermark evasion method using the Deep Image Prior (DIP) (Ulyanov et al., 2018)—an untrained DNN-based prior that proves powerful in solving single-image blind denoising and numerous single-instance inverse problems (Qayyum et al., 2023; Tirer et al., 2023; Zhuang, 2023). Our main contributions include: **(i)** We show that DIP-based blind denoising can be used to generate high-quality evasion images effective against many existing invisible watermarks, both training-based and manually designed; **(ii)** We elucidate the principle behind DIP’s evasion performance—its faster rate in picking up low frequencies than high ones empowers its image-agnostic watermark purification ability. Due to **(i)** and **(ii)**, we advocate including DIP evasion as an integral component in the robustness evaluation of watermarking systems (Saberi et al., 2023; An et al., 2024); **(iii)** Based on our analysis, we further recommend that to counteract black-box watermark evasions, a reliable watermark scheme should focus on modifying low-frequency components and have a reasonable magnitude.

2 Background and related work

(Blind) image steganography refers to the technique of hiding secret but retrievable messages in an image with minimal change to the image (Zhu et al., 2018). Given an arbitrary natural image $I \in \mathcal{I}$, where \mathcal{I} denotes the set of natural images, and an arbitrary n -bit message $\mathbf{w} \in \{0, 1\}^n$, an image steganography system typically consists of an encoder E —which takes any image I and any message \mathbf{w} and produces an encoded image, a decoder D —which takes any image and produces an informative message, and its system goal: (\circ means function composition)

$$(D \circ E)(I, \mathbf{w}) = \mathbf{w}, \quad \forall I \in \mathcal{I}, \forall \mathbf{w} \in \{0, 1\}^n, \quad (\text{correctly encode and decode } \mathbf{w}) \quad (1a)$$

$$D(I) = \emptyset, \quad \forall I \in \mathcal{I}, \quad (\text{no useful message decoded from a clean image}) \quad (1b)$$

$$E(I, \mathbf{w}) \approx I, \quad \forall I \in \mathcal{I}, \forall \mathbf{w} \in \{0, 1\}^n. \quad (\text{minimal encoding distortion to the image}) \quad (1c)$$

Existing steganography methods differ by whether the encoder and decoder are manually designed or learned from data. Manually designed encoder-decoder pairs rely on ideas such as manipulating the least significant bit (LSB) (Tirkel et al., 1993), template matching in the Fourier domain (Pereira & Pun, 2000), discrete wavelet transform (DWT), discrete cosine transform (DCT), and singular value decomposition (SVD) (Bi et al., 2007; Pereira & Pun, 2000; Navas et al., 2008). In contrast, training-based methods often learn DNN-based encoder-decoder pairs from data, based on variants of a model formulation derived from the goal stated in Eq. (1):

$$\begin{aligned} \min_{\phi, \theta} \mathbb{E}_{\mathbf{w}, I} \ell_m[\mathbf{w}, (D_{\theta} \circ E_{\phi})(I, \mathbf{w})] & \quad (\text{to ensure Eq. (1a)}) \\ \text{s. t. } \ell_q(I, E_{\phi}(I, \mathbf{w})) \leq \delta, \quad \forall I \in \mathcal{I}, \forall \mathbf{w} \in \{0, 1\}^n, & \quad (\text{to ensure Eq. (1c)}) \end{aligned} \quad (2)$$

where ϕ and θ are learnable weights of the DNNs in E and D , respectively; ℓ_m and ℓ_q are two losses measuring the error of **message recovery** and the **quality distortion** to the image, respectively; and δ is the maximally allowed perturbation to the image caused by watermarking embedding. Representative training-based methods include HIDDEN and its variants (Zhu et al., 2018; Wen & Aydore, 2019; Luo et al., 2020), SteganoGAN (Zhang et al., 2019a), Stable Signature (Fernandez et al., 2023), rivaGAN (Zhang et al., 2019b), StegaStamp (Tancik et al., 2020), Mbrs (Jia et al., 2021) and TrustMark (Bui et al., 2023a). These methods typically also incorporate regularization terms to encourage the distribution of the encoded images to be close to that of the original images based on generative adversarial networks (GAN) (Goodfellow et al., 2014a). SSL (Fernandez et al., 2022) and RoSteALS (Bui et al., 2023b) are similar in spirit but perform learning in different spaces. In theory, solving Eq. (2) with a reasonably small δ can always produce distortion patterns that are *invisible* to human eyes. However, existing methods typically work with heuristic penalty or regularization forms of

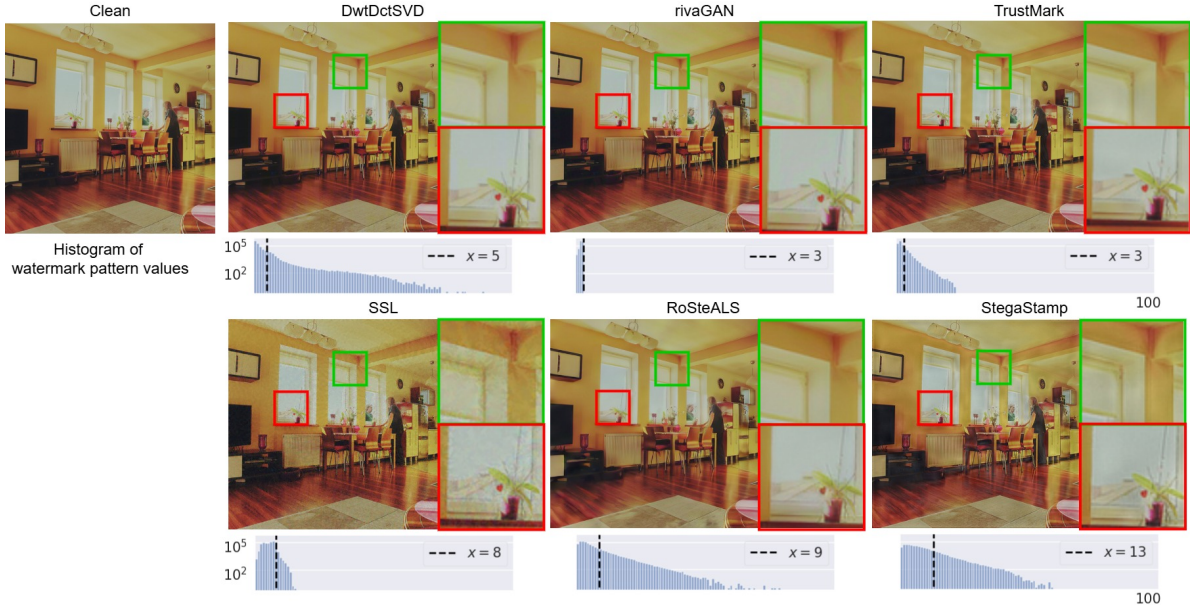


Figure 3: Visualization of a clean image (from COCO) and its steganography versions by different methods. Below each steganography image is the histogram of the pixel magnitude in the corresponding distortion (i.e., difference between the steganography image and the clean image): y -axis is in log scale and the vertical dashed line marks the 90% quantile. While DwtDctSVD, rivaGAN and TrustMark induce distortions that are almost invisible, SSL, RoSteALS and StegaStamp produce relatively more visible distortions—local color jitters for SSL, global color jitters for StegaStamp, and global smoothing for RoSteALS. All images presented above are in `uint8` format with value in $[0, 255]$ with resolution 512×512 .

Eq. (2) and therefore do not necessarily find feasible solutions to Eq. (2), e.g., (Zhu et al., 2018). In addition, the choice of ℓ_q can differ, e.g., mean squared error (MSE) (Zhu et al., 2018; Zhang et al., 2019a), LPIPS distance (Zhang et al., 2018). Therefore, different methods lead to different levels of visible distortions. Fig. 3 visualizes several popular training-based methods (together with the manually designed DwtDctSVD) and highlights the different distortion levels that they lead to.

(Blind) image watermarking Based on steganography, a natural way to trace AI-generated images is to assign a *fixed message* \mathbf{w} as the signature of the content owner (e.g., a company) and apply steganography to generate images containing the signature, i.e., watermarked images, to achieve (Jiang et al., 2023):

$$D(E(I, \mathbf{w})) = \mathbf{w}, \quad \forall I \in \mathcal{I}, \quad (\mathbf{w} \text{ is a fixed message representing the signature}) \quad (3a)$$

$$D(I) \neq \mathbf{w}, \quad \forall I \in \mathcal{I}, \quad (\text{messages decoded from unwatermarked images should not be } \mathbf{w}) \quad (3b)$$

$$E(I, \mathbf{w}) \approx I, \quad \forall I \in \mathcal{I}. \quad (\text{minimal encoding distortion to the image}) \quad (3c)$$

In practice, whether an image I is watermarked by \mathbf{w} can be detected by comparing the decoded message with \mathbf{w} :

$$\mathbb{1}[BA(D(I), \mathbf{w}) > \gamma], \quad (4)$$

where BA denotes the bitwise accuracy and γ is a preset task-dependent threshold (Jiang et al., 2023; Fernandez et al., 2023; Yu et al., 2021). Due to the similarity between Eq. (3) and Eq. (1), most existing work considers image watermarking as a special application of steganography, e.g., Zhu et al. (2018); Tancik et al. (2020); An et al. (2024); Zhao et al. (2024). As a result, the learning formulation in Eq. (2) is also widely adopted in works that only focus on watermarking systems, e.g., Zhang et al. (2019b); Fernandez et al. (2023).

The above watermark methods are *post-processing* in nature, as the watermark is embedded on any given image I that is already generated. There is an emerging line of *in-processing* watermark methods that directly modify the image generation process (Zhao et al., 2024; An et al., 2024), including TreeRing watermark (Wen

et al., 2023), stable signature (Fernandez et al., 2023), Gaussian shading watermark (Yang et al., 2024), and pseudorandom error-correcting code watermark Gunn et al. (2024). In these in-processing methods, there is no notion of “clean images” I and every generated watermark image exhibits a semantic shift compared to the image generated without the in-process watermarking; see Fig. 4 for an example generated by the TreeRing watermark. **In this paper, we focus on post-processing watermark methods due to their flexibility, as they are agnostic to the image generation process.**

Robustness of watermarking systems Robustness of an image watermarking system refers to the extent of the watermark to remain detectable by the decoder D when the watermarked image is manipulated (also called “evaded” if such manipulation is a deliberate attack). Thus, robustness is typically associated with the potential of a watermarking system to be applied to copyright protection and misinformation detection. To stress test the robustness of watermark systems, various watermark evasion techniques have been proposed. These techniques are broadly classified into white-box and black-box evasions, depending on whether any component of the watermark system is known to the evader (An et al., 2024). **In this paper, we focus on black-box evasions where nothing about the watermark**



Figure 4: Visualization of a TreeRing watermark example, where (a) and (b) are images generated from the same text prompt input using the same image diffusion model without and with the in-process watermarking, respectively.

system is known, as in practice, companies tend to keep their watermark system private. Existing black-box evasions can be classified into two groups: **Corruption methods** try to distort watermarked images so that watermarks become corrupted and undetectable. Classical digital editing (e.g., applying Gaussian noise, Gaussian blur, JPEG compression, etc. (Voyatzis & Pitas, 1999)), the query-based adversarial attack (WevadeBQ) in Jiang et al. (2023) and the surrogate attack in Saberi et al. (2023) belong to this group; **Purification methods** treat embedded watermark patterns as noise signals and attempt to remove them using denoising and regeneration techniques, such as BM3D (Dabov et al., 2007), diffusion models (Saberi et al., 2023; Zhao et al., 2023) and VAE (Zhao et al., 2023). The rationale behind the purification methods is rooted in Eq. (3), where the original image, if recovered successfully, is always an evasion. In addition, the original image will be the ultimate threat to any watermarking system—the watermark is evaded by an image without any loss of quality.

3 Our method: DIP for black-box watermark evasion

3.1 Watermark evasion via DIP-based blind denoising

Deep Image Prior (DIP) refers to the technique of using **untrained** DNN as an implicit prior for natural images in solving image recovery problems, **without training on massive data**: for any natural image I , DIP parametrizes it as $I = G_{\theta}(z)$, where G_{θ} is typically a trainable convolutional neural network (CNN) and z is a fixed input (typically randomly drawn). Now consider the canonical optimization-based formulation for image recovery problems:

$$\min_I \ell(\mathbf{y}, f(I)) + \lambda R(I), \quad (5)$$

where $\mathbf{y} \approx f(I)$ is the observation model, $\ell(\mathbf{y}, f(I))$ measures the recovery error, and $R(\cdot)$ denotes regularization on I . DIP transforms the formulation into

$$\min_{\theta} \ell(\mathbf{y}, f(G_{\theta}(z))) + \lambda R(G_{\theta}(z)). \quad (6)$$

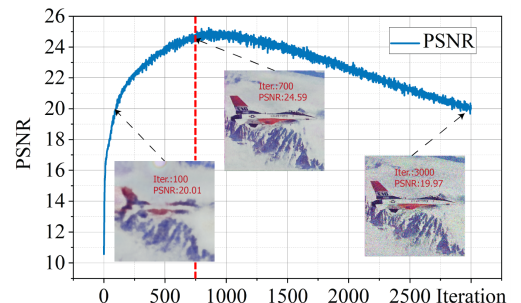


Figure 5: A typical image quality (measured by peak signal-to-noise ratio, PSNR) vs. iteration curve when DIP is used in blind denoising tasks. An early stopping method is used to detect the iteration achieving the peak performance (red dashed line). (Figure adapted from Wang et al. (2021) under the Creative Commons 4.0 license)

Note that the optimization is *only* with respect to the CNN weights θ . The resulting formulation is then solved by first-order optimizers, such as ADAM (Kingma & Ba, 2014). Such a simple strategy, in combination with appropriate early stopping methods (Li et al., 2021; Wang et al., 2021; Shi et al., 2022b) that pick the best intermediate recovered images, has proved highly successful in solving a wide range of image recovery problems, from simple denoising (Ulyanov et al., 2018) to advanced scientific and medical reconstruction problems (Tirer et al., 2023; Qayyum et al., 2023; Zhuang, 2023; Zhuang et al., 2024; 2023; Li et al., 2024; 2023b;a).

Algorithm 1 DIP-based watermark evasion

Require: A single watermarked image I_w ; a CNN $G_\theta(\mathbf{z})$ where θ collects the trainable parameters and \mathbf{z} is a fixed vector (randomly drawn as iid Gaussian); a watermark detection API whose input can be an arbitrary image and returns “Yes/No” as the detection output.

- 1: Randomly initialize $\theta^{(0)}$
 - 2: Solve $\min_{\theta} \ell_2(I_w, G_\theta(\mathbf{z}))$ using the ADAM optimizer for a sufficient number of iterations N ; record all intermediate results $I_i = G_{\theta^{(i)}}(\mathbf{z})$, $\forall i \leq N$, where i denotes the iteration number.
 - 3: Query the detection API using all I_i ’s; return all I_i ’s that have no watermark detected.
-

Watermark evasion via DIP-based blind denoising Now, consider an arbitrary watermarked image $I_w \doteq E(I, \mathbf{w})$, where we do not know E or \mathbf{w} . Since $I_w \approx I$ as required in Eq. (3) and I is clearly a successful invasion, it is sensible to try to “purify” or “denoise” I_w toward I —the intuition behind all purification methods for black-box evasion (Dabov et al., 2007; Saberi et al., 2023; Zhao et al., 2023).

DIP has proven effective in single-image denoising, e.g., with Gaussian, impulse, shot noise, etc., when combined with appropriate early stopping strategies (Mataev et al., 2019; Jo et al., 2021; Li et al., 2021; Wang et al., 2021; Li et al., 2023a;b; 2024). In particular, when the noise level is low—which is true for typical watermarking systems as I_w is supposed to be very close to I , a simple formulation with the standard mean-squared-error (MSE) loss and the additive noise model can perform “blind” simultaneous denoising for multiple types of noise Li et al. (2021); Wang et al. (2021). Inspired by this, we propose a simple DIP-based blind watermark-evasion formulation

$$\min_{\theta} \|I_w - G_\theta(\mathbf{z})\|_2^2, \quad (\text{DIP-based watermark evasion}) \quad (7)$$

for any given watermarked image I_w . Unlike DIP-based blind denoising which requires appropriate early stopping strategies to find optimal denoising, we only need to check the evasion success of all iterates when iteratively solving Eq. (7) by querying the watermark decoder. Our whole algorithm pipeline is summarized in Algorithm 1. While we do not invent DIP-based blind denoising, we are the first to explore it for blind evasion of invisible watermarks. Rishik also performs DIP-based watermark removal, but solves it as *image inpainting* which requires **known watermark patterns and locations**.

3.2 Why including DIP-based evasion as a baseline method?

The primary obstacle for purification methods is that the “noise” patterns induced by watermark methods, especially those training-based ones, may not follow any simple noise model. Consequently, classical denoising methods that target specific noise types, such as BM3D, may struggle to remove the watermark. The recent regeneration techniques via diffusion models or VAE effectively perform learned denoising. However, a priori, it is unclear they can generalize well to novel watermark patterns. **In contrast, our DIP-based evasion operates on a different principle:** it leverages the different rates at which different frequency components are captured during DIP learning through Eq. (7), which has been consistently observed in prior DIP literature (Ulyanov et al., 2018; Shi et al., 2022a; Li et al., 2021; Wang et al., 2021). Specifically, the $G_\theta(\mathbf{z})$ term in Eq. (7) picks up the low-frequency components—which dominate natural images, **much faster** than picking up the high-frequency components—which tend to be noise-induced, likely watermark-induced for our case.

- In Fig. 6, we compare the Fourier spectrum of the clean image from Fig. 3 to those of various watermarked versions: clearly, the spectrum of the clean image concentrates on low frequencies, but different watermark

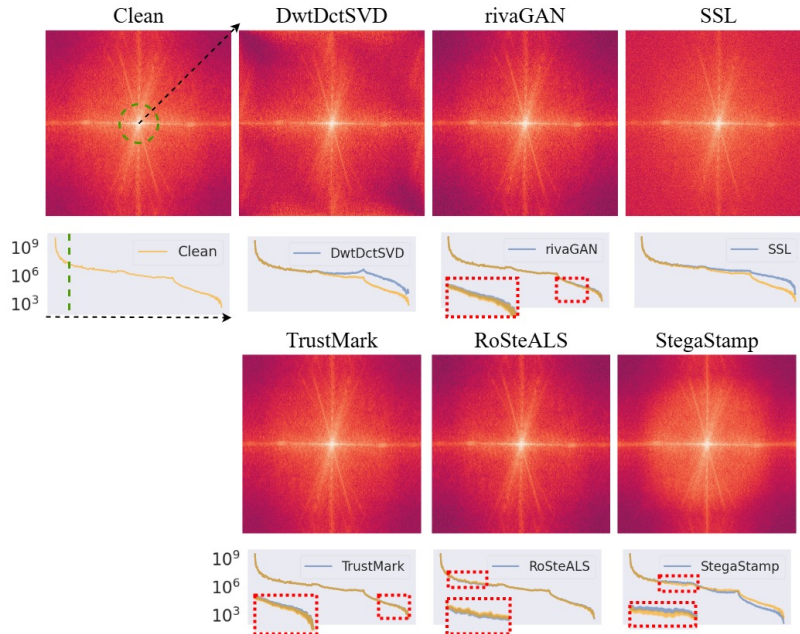


Figure 6: Visualization of 2D Fourier spectra of the clean and watermarked images from Fig. 3 (magnitudes visualized in log scale). The histogram below each spectrum plot shows the band-wise energy distribution in the radial direction (i.e., the dashed arrow direction), where the y -axis is in log scale.

methods reshape the Fourier spectrum by mostly changing the mid-to-high frequencies. For example, RoSteALS and StegaStamp mostly affect the low-mid frequencies, DwtDctSVD and SSL mostly focus on mid-high frequencies, and rivaGAN alters high frequencies. The only exception is TrustMark, whose watermark pattern is hard to observe from the frequency spectrum.

- Next, in Fig. 7, we visualize the different learning paces of DIP across different frequency bands, by tracking the frequency band errors (FBEs) similar to Wang et al. (2024); Li et al. (2023a); Zhuang et al. (2024): we first compute the relative per-frequency error in the frequency domain, i.e., $|\mathcal{F}(I_w) - \mathcal{F}(G_{\theta^{(i)}})|/|\mathcal{F}(I_w)|$, where $\mathcal{F}(\cdot)$ is the discrete Fourier transform, then divide all frequencies into five radial bands from the lowest (1) to the highest (5), and compute the mean errors within each band. It is evident that the lower the frequencies, the faster the FBEs decay.

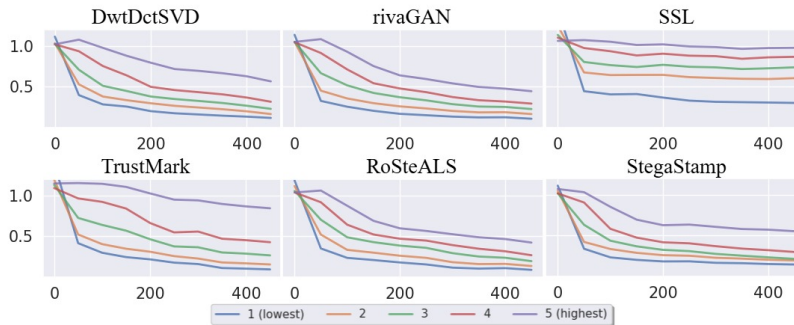


Figure 7: Evolution of the Fourier band errors (FBEs) of DIP's intermediate iterates (x -axis: iteration count; y -axis: relative band error). We visualize FBEs by dividing all frequency components into five different bands in the radial direction, from the lowest (1) to highest (5).

Such disparate learning paces imply that certain intermediate iterates enjoy sufficient separation of the low-frequency image content and high-frequency watermark patterns, hence the potential for successful evasion. In summary, compared to alternative purification methods that depend on either explicit noise modeling or data-driven priors, our DIP-based evasion relies on frequency separation that is noise-agnostic and distribution-free. Hence, our DIP-based evasion method largely complements the existing ones.

3.3 Remarks on improving the query efficiency

Algorithm 1 often takes up to ~ 1000 iterative steps to solve Eq. (7). Querying the decoder using all intermediate iterates, as described in Algorithm 1, may be costly, and the decoder server may also limit query frequency for individual users to ensure safety and fairness. To reduce the number of queries and

Table 1: Quantitative visual distortion induced by different watermark methods. We report the mean and standard deviation (in parathesis) of all three quality metrics, calculated over 100 randomly drawn test images. All images are in `uint8` format with value in $[0, 255]$. RivaGAN has the least visible watermarks, while StegaStamp has the most.

Watermark	COCO dataset			DiffusionDB dataset		
	PSNR \uparrow	SSIM \uparrow	90% Quantile \downarrow	PSNR \uparrow	SSIM \uparrow	90% Quantile \downarrow
DwtDctSVD	38.31 (2.67)	0.98 (0.01)	4.66 (0.90)	37.88 (3.60)	0.97 (0.02)	4.87 (1.56)
rivaGAN	40.57 (0.21)	0.98 (0.01)	3.00 (0.03)	40.61 (0.24)	0.98 (0.01)	3.00 (0.03)
SSL	33.03 (0.23)	0.88 (0.04)	7.19 (0.74)	33.14 (0.55)	0.88 (0.04)	7.10 (0.72)
TrustMark	40.46 (1.85)	0.99 (0.01)	3.84 (0.85)	40.67 (2.62)	0.99 (0.01)	3.84 (1.14)
RoSteALS	30.83 (2.71)	0.95 (0.02)	12.8 (3.98)	30.88 (4.12)	0.95 (0.03)	12.5 (5.71)
StegaStamp	28.34 (1.61)	0.90 (0.03)	15.9 (3.18)	26.58 (2.01)	0.84 (0.04)	19.3 (4.96)

thereby improve query efficiency, it makes sense to only send high-quality iterates to the decoder—again, we emphasize both image quality and evasion success in this paper. To this end, although the clean image I is unknown, the watermarked image I_w is very close to I by design (i.e., per Eq. (3)). Therefore, we can take I_w as a proxy reference to estimate the image quality of intermediate iterates; see Appendix C for exemplar trajectories of image quality and watermark detectability on different watermarks by different evasion methods.

4 Qualitative and quantitative evaluation

Experiment setup **(1) Datasets:** We use images from two large-scale datasets: **(i)** MS-COCO (Lin et al., 2014) composed of 328K real images and **(ii)** DiffusionDB (Wang et al., 2022) composed of 14 million high-quality AI-generated images. We randomly sample 2000 images from each dataset—the typical scale for the robustness evaluation of watermark systems (An et al., 2024), resize them to 512×512 , and generate images with different watermarks, respectively; **(2) Watermark methods:** We focus on 6 representative and publicly available *post-processing* watermark methods: DwtDctSVD, rivaGAN, SSL, TrustMark, RoSteALS, and StegaStamp, whose watermark patterns vary in the visibility level and Fourier spectrum; see Figs. 3 and 6 and Table 1 for visual and quantitative comparisons, respectively. We also evaluate on the SOTA *in-processing* TreeRing watermark, where 2000 watermarked images are generated using *Gustavosta* stable diffusion prompts from HuggingFace (Santana); **(3) Evasion methods:** In addition to our DIP-based evasion method described in Algorithm 1, ² we also consider the following classical digital editing methods: **(i)** brightness, **(ii)** contrast, **(iii)** Gaussian noise, **(iv)** JPEG compression, **(v)** bm3d denoising, and recent SOTA purification methods: **(vi)** DiffPure (Saber et al., 2023), **(vii)** Diffuser and **(viii)** VAE regeneration (Jiang et al., 2023)³.

Evaluation protocol As we argue in Section 1 (see also An et al. (2024)), evasion success and image quality are two essential dimensions of watermarking systems. Therefore, we report the *best image quality* each evasion method can achieve while failing watermark detection. To find the “optimal” tradeoff image, we perform an exhaustive search over the allowable ranges of the hyperparameters for each evasion method and look for images with **(i)** watermark undetected and **(ii)** the highest PSNR value with respect to the watermarked image I_w ; see Section 3.3 for justification on why I_w is used and Appendix B for details about all hyperparameters. Finally, to quantify the quality of such images, we use three metrics: **(i)** PSNR, **(ii)** Structural Similarity Index Measure (SSIM) (Hore & Ziou, 2010) and **(iii)** 90% quantile of pixel-wise difference, all with respect to the clean image I . The quantile metric mainly serves as a supplement, as PSNR and SSIM focus on the average difference while it reflects the difference on the tail—watermark-induced distortion to an image may be highly localized and hence spatially sparse, which might not be captured by averaging metrics; see Fig. 3 and Table 1 for a sense of the visual and quantitative distortions caused by different watermark methods. Since the TreeRing watermark lacks a notion of clean image, we use I_w as the reference in all evaluation experiments related to TreeRing watermark.

²We use the default ‘skip’ network in the original DIP repo: <https://github.com/DmitryUlyanov/deep-image-prior>.

³VAE regeneration using model from Cheng et al. (2020), which gives the best VAE performance as in Jiang et al. (2023).

Table 2: The best image quality produced by different evasion methods under different detection threshold γ on the COCO dataset. Here, we report the mean value of PSNR-SSIM-90% Quantile (Q.). We highlight the best evasion method under each watermark and γ in **boldface**. For fair comparison, we mask out cases where one evasion method cannot evade $\geq 90\%$ of the watermarked images.

COCO dataset		$\gamma = 0.55$	$\gamma = 0.65$	$\gamma = 0.75$	$\gamma = 0.85$
DwtDctSVD	TPR \uparrow / FPR \downarrow	1.00 / 0.23	0.99 / 0.03	0.99 / 0.01	0.99 / 0.00
brightness	PSNR - SSIM - Q.	19.22 - 0.88 - 52.6	20.00 - 0.90 - 47.5	20.67 - 0.91 - 43.4	21.52 - 0.93 - 39.0
contrast		25.27 - 0.89 - 26.7	26.02 - 0.91 - 24.1	26.67 - 0.91 - 22.0	27.52 - 0.92 - 19.7
Gaussian noise		16.30 - 0.19 - 66.1	17.54 - 0.23 - 56.8	18.62 - 0.26 - 50.3	20.05 - 0.31 - 42.3
JPEG		31.52 - 0.88 - 11.2	31.74 - 0.89 - 10.9	31.89 - 0.89 - 10.7	32.13 - 0.90 - 10.4
bm3d		****	****	**	30.26 - 0.87 - 9.6
DiffPure		28.20 - 0.79 - 17.3	29.61 - 0.83 - 14.2	29.90 - 0.84 - 13.6	29.94 - 0.84 - 13.6
Diffuser		**	**	*25.87 - 0.74 - 20.7	26.61 - 0.76 - 19.2
VAE		****	*32.38 - 0.88 - 10.5	33.47 - 0.90 - 9.2	34.51 - 0.92 - 8.1
DIP (ours)		34.87 - 0.96 - 7.2	35.50 - 0.96 - 6.7	35.85 - 0.96 - 6.4	36.22 - 0.97 - 6.1
rivaGAN	TPR \uparrow / FPR \downarrow	0.99 / 0.25	0.99 / 0.03	0.99 / 0.01	0.99 / 0.00
brightness	PSNR - SSIM - Q.	****	6.91 - 0.12 - 181	7.31 - 0.17 - 173	8.02 - 0.27 - 159
contrast		****	*13.16 - 0.50 - 90.0	13.53 - 0.53 - 86.1	14.20 - 0.58 - 79.8
Gaussian noise		11.06 - 0.07 - 121	13.07 - 0.11 - 96.3	14.61 - 0.14 - 80.7	16.42 - 0.19 - 65.7
JPEG		****	**	28.22 - 0.79 - 16.7	30.16 - 0.85 - 13.2
bm3d		****	****	****	****
DiffPure		*26.51 - 0.73 - 21.7	28.84 - 0.80 - 15.9	29.72 - 0.83 - 14.1	29.96 - 0.84 - 13.5
Diffuser		****	*25.40 - 0.72 - 22.1	*26.28 - 0.74 - 20.0	26.78 - 0.75 - 18.9
VAE		**	*32.34 - 0.88 - 10.3	33.28 - 0.90 - 9.3	34.21 - 0.91 - 8.3
DIP (ours)		29.87 - 0.87 - 17.8	32.64 - 0.92 - 11.1	34.02 - 0.94 - 8.9	35.20 - 0.95 - 7.4
SSL	TPR \uparrow / FPR \downarrow	1.00 / 0.33	1.00 / 0.07	0.99 / 0.01	0.99 / 0.00
brightness	PSNR - SSIM - Q.	****	****	****	*13.92 - 0.44 - 149
contrast		****	****	**	*19.12 - 0.67 - 58.6
Gaussian noise		*18.89 - 0.28 - 51.4	21.67 - 0.39 - 36.7	23.98 - 0.48 - 27.8	25.42 - 0.54 - 22.7
JPEG		*28.18 - 0.79 - 16.7	30.05 - 0.84 - 13.4	31.28 - 0.86 - 11.4	32.73 - 0.89 - 9.5
bm3d		*27.99 - 0.79 - 14.4	29.59 - 0.84 - 11.7	30.79 - 0.87 - 9.6	31.18 - 0.89 - 8.9
DiffPure		27.18 - 0.75 - 19.7	28.85 - 0.80 - 15.6	29.32 - 0.82 - 14.6	29.38 - 0.82 - 14.4
Diffuser		**	*25.39 - 0.68 - 22.1	*25.80 - 0.69 - 21.1	*25.90 - 0.69 - 20.8
VAE		* 31.21 - 0.85 - 11.9	* 32.03 - 0.88 - 10.8	32.83 - 0.90 - 9.8	33.50 - 0.91 - 9.0
DIP (ours)		23.73 - 0.76 - 31.4	28.21 - 0.85 - 17.4	31.46 - 0.90 - 11.2	33.64 - 0.92 - 8.4
TrustMark	TPR \uparrow / FPR \downarrow	1.00 / 0.13	1.00 / 0.00	1.00 / 0.00	1.00 / 0.00
brightness	PSNR - SSIM - Q.	****	**	*6.86 - 0.11 - 182	*7.27 - 0.17 - 173
contrast		****	**	*13.31 - 0.54 - 88.3	*13.84 - 0.58 - 88.2
Gaussian noise		9.57 - 0.05 - 144	11.17 - 0.07 - 119	12.72 - 0.09 - 99.0	14.49 - 0.13 - 80.9
JPEG		****	****	*25.18 - 0.70 - 22.9	*26.35 - 0.73 - 20.4
bm3d		—	—	—	—
DiffPure		26.34 - 0.73 - 20.4	27.81 - 0.77 - 17.3	29.09 - 0.80 - 15.3	30.22 - 0.84 - 13.2
Diffuser		****	*25.62 - 0.74 - 21.1	*26.19 - 0.75 - 19.7	26.70 - 0.77 - 18.5
VAE		—	—	****	****
DIP (ours)		**	*13.64 - 0.48 - 91.1	15.88 - 0.56 - 73.4	18.97 - 0.66 - 52.8
RoSteALS	TPR \uparrow / FPR \downarrow	1.00 / 0.29	1.00 / 0.01	1.00 / 0.00	1.00 / 0.00
brightness	PSNR - SSIM - Q.	—	—	—	—
contrast		—	—	—	—
Gaussian noise		—	****	****	*9.53 - 0.04 - 145
JPEG		—	—	—	****
bm3d		—	—	—	—
DiffPure		* 19.12 - 0.49 - 50.6	22.98 - 0.62 - 30.7	24.91 - 0.69 - 24.3	26.28 - 0.74 - 20.6
Diffuser		—	—	—	****
VAE		—	—	—	—
DIP (ours)		****	*11.08 - 0.38 - 113	12.09 - 0.42 - 105	16.36 - 0.56 - 73.5
StegaStamp	TPR \uparrow / FPR \downarrow	1.00 / 0.18	1.00 / 0.01	1.00 / 0.00	1.00 / 0.00
brightness	PSNR - SSIM - Q.	—	—	—	—
contrast		—	—	****	*13.22 - 0.52 - 88.9
Gaussian noise		****	*7.83 - 0.03 - 175	9.26 - 0.05 - 148	11.24 - 0.08 - 118
JPEG		****	****	****	**
bm3d		—	—	—	—
DiffPure		19.57 - 0.50 - 45.6	22.42 - 0.61 - 31.5	23.81 - 0.66 - 26.7	24.67 - 0.70 - 24.1
Diffuser		—	—	****	**
VAE		—	—	—	—
DIP (ours)		**	*12.29 - 0.40 - 102	14.00 - 0.47 - 87.5	16.05 - 0.55 - 70.9

The following markers are used for the purpose of fair comparison of the best evasion image quality:

— Evasion method only successfully evade < 10% of the watermarked images.

**** Evasion method only successfully evade < 75% of the watermarked images.

** Evasion method only successfully evade < 90% of the watermarked images.

* Evasion method successfully evade $\geq 90\%$ of the watermarked images, but < 100%.

Table 3: The best image quality produced by different evasion methods under different detection threshold γ on the DiffusionDB dataset. Here, we report the mean value of PSNR-SSIM-90% Quantile (Q.). We highlight the best evasion method under each watermark and γ in **boldface**. For fair comparison, we mask out cases where one evasion method cannot evade $\geq 90\%$ of the watermarked images.

DiffusionDB dataset		$\gamma = 0.55$	$\gamma = 0.65$	$\gamma = 0.75$	$\gamma = 0.85$
DwtDctSVD	TPR \uparrow / FPR \downarrow	1.00 / 0.23	0.99 / 0.03	0.99 / 0.01	0.99 / 0.00
brightness	PSNR - SSIM - Q.	21.25 - 0.90 - 43.0	21.94 - 0.91 - 39.1	22.54 - 0.92 - 35.9	23.34 - 0.93 - 32.3
contrast		26.89 - 0.91 - 22.2	27.56 - 0.92 - 20.1	28.11 - 0.93 - 18.6	28.85 - 0.94 - 16.8
Gaussian noise		16.52 - 0.22 - 64.3	17.73 - 0.25 - 55.5	18.81 - 0.29 - 49.1	20.07 - 0.33 - 42.0
JPEG		30.47 - 0.86 - 13.2	30.81 - 0.87 - 12.7	31.00 - 0.88 - 12.4	31.30 - 0.88 - 12.0
bm3d		****	****	**	*28.94 - 0.85 - 11.6
DiffPure		27.69 - 0.78 - 18.8	29.09 - 0.82 - 15.8	29.52 - 0.83 - 15.0	29.56 - 0.83 - 14.9
Diffuser		**	**	*25.88 - 0.75 - 21.7	*26.54 - 0.77 - 20.5
VAE		****	*31.91 - 0.87 - 11.5	32.90 - 0.89 - 10.3	32.92 - 0.91 - 9.0
DIP (ours)		35.29 - 0.96 - 6.9	35.91 - 0.96 - 6.4	36.25 - 0.97 - 6.1	36.53 - 0.97 - 5.9
rivaGAN	TPR \uparrow / FPR \downarrow	0.99 / 0.25	0.99 / 0.03	0.99 / 0.01	0.99 / 0.00
brightness	PSNR - SSIM - Q.	****	*7.38 - 0.13 - 173	7.83 - 0.19 - 165	8.70 - 0.31 - 150
contrast		****	*13.47 - 0.51 - 86.8	13.93 - 0.55 - 82.5	14.73 - 0.60 - 75.5
Gaussian noise		10.96 - 0.08 - 123	12.98 - 0.12 - 97.3	14.55 - 0.16 - 81.4	16.56 - 0.21 - 64.8
JPEG		****	*26.31 - 0.74 - 20.9	*27.84 - 0.79 - 17.5	29.61 - 0.84 - 14.1
bm3d		****	****	****	****
DiffPure		26.11 - 0.73 - 22.9	28.25 - 0.79 - 16.8	28.88 - 0.81 - 15.4	29.02 - 0.82 - 15.1
Diffuser		****	*25.43 - 0.73 - 22.5	*26.12 - 0.75 - 20.8	26.47 - 0.76 - 20.0
VAE		**	*32.29 - 0.88 - 10.4	*33.13 - 0.90 - 9.4	33.94 - 0.91 - 8.5
DIP (ours)		31.91 - 0.89 - 14.5	34.48 - 0.93 - 9.1	35.72 - 0.95 - 7.4	36.75 - 0.96 - 6.2
SSL	TPR \uparrow / FPR \downarrow	1.00 / 0.33	1.00 / 0.07	0.99 / 0.01	0.99 / 0.00
brightness	PSNR - SSIM - Q.	****	****	**	*16.91 - 0.53 - 97.9
contrast		****	****	**	*21.54 - 0.73 - 47.9
Gaussian noise		*17.43 - 0.26 - 63.8	20.90 - 0.38 - 41.0	23.48 - 0.48 - 29.7	25.31 - 0.56 - 23.0
JPEG		*27.07 - 0.77 - 19.4	28.97 - 0.82 - 15.4	30.47 - 0.85 - 12.7	32.39 - 0.89 - 9.9
bm3d		*26.69 - 0.77 - 16.3	28.00 - 0.82 - 13.3	29.00 - 0.85 - 11.1	29.25 - 0.86 - 10.5
DiffPure		26.67 - 0.75 - 21.0	28.05 - 0.79 - 17.3	28.40 - 0.80 - 16.3	28.43 - 0.80 - 16.2
Diffuser		**	*25.00 - 0.68 - 23.6	25.43 - 0.69 - 22.5	25.49 - 0.70 - 22.4
VAE		* 30.26 - 0.85 - 12.3	* 31.79 - 0.88 - 11.0	32.43 - 0.90 - 9.9	33.01 - 0.91 - 9.2
DIP (ours)		23.14 - 0.72 - 35.2	27.95 - 0.84 - 18.2	31.27 - 0.89 - 11.8	33.84 - 0.92 - 8.2
TrustMark	TPR \uparrow / FPR \downarrow	1.00 / 0.13	1.00 / 0.00	1.00 / 0.00	1.00 / 0.00
brightness	PSNR - SSIM - Q.	****	**	*7.09 - 0.10 - 179	*7.43 - 0.15 - 172
contrast		****	**	*13.52 - 0.55 - 87.3	*13.98 - 0.59 - 83.2
Gaussian noise		*9.62 - 0.05 - 143	11.17 - 0.08 - 119	12.67 - 0.10 - 100	14.45 - 0.14 - 81.7
JPEG		****	****	*25.06 - 0.69 - 24.5	*26.08 - 0.72 - 22.4
bm3d		---	---	---	---
DiffPure		26.60 - 0.73 - 21.8	27.91 - 0.77 - 18.7	28.99 - 0.79 - 16.6	30.07 - 0.83 - 14.4
Diffuser		**	*25.79 - 0.74 - 21.9	*26.40 - 0.76 - 20.4	26.96 - 0.77 - 19.2
VAE		---	---	****	****
DIP (ours)		**	*14.16 - 0.5 - 88.4	16.19 - 0.57 - 73.0	19.07 - 0.65 - 54.6
RoSteALS	TPR \uparrow / FPR \downarrow	1.00 / 0.29	1.00 / 0.01	1.00 / 0.00	1.00 / 0.00
brightness	PSNR - SSIM - Q.	---	---	---	---
contrast		---	---	---	---
Gaussian noise		---	****	****	*9.92 - 0.05 - 139
JPEG		---	---	---	****
bm3d		---	---	---	---
DiffPure		20.86 - 0.57 - 43.7	24.06 - 0.66 - 29.3	25.74 - 0.72 - 23.8	26.93 - 0.76 - 20.6
Diffuser		---	---	---	****
VAE		---	---	---	---
DIP (ours)		**	*11.67 - 0.42 - 108	12.83 - 0.46 - 98.9	17.47 - 0.60 - 67.0
StegaStamp	TPR \uparrow / FPR \downarrow	1.00 / 0.18	1.00 / 0.01	1.00 / 0.00	1.00 / 0.00
brightness	PSNR - SSIM - Q.	---	---	---	---
contrast		---	---	****	**
Gaussian noise		****	*8.03 - 0.04 - 170	9.49 - 0.06 - 145	11.66 - 0.09 - 113
JPEG		****	****	****	**
bm3d		---	---	---	---
DiffPure		* 19.70 - 0.54 - 45.6	22.42 - 0.63 - 32.2	23.73 - 0.68 - 27.5	24.55 - 0.71 - 24.9
Diffuser		---	---	****	*21.97 - 0.61 - 32.4
VAE		---	---	---	---
DIP (ours)		**	*13.01 - 0.44 - 96.7	14.69 - 0.50 - 82.7	16.54 - 0.57 - 68.5

The following markers are used for the purpose of fair comparison of the best evasion image quality:

— Evasion method only successfully evade < 10% of the watermarked images.

**** Evasion method only successfully evade < 75% of the watermarked images.

** Evasion method only successfully evade < 90% of the watermarked images.

* Evasion method successfully evade $\geq 90\%$ of the watermarked images, but < 100%.

Table 4: The best image quality produced by different evasion methods under different detection threshold on Tree-Ring watermarked images. Here, we report the mean value of PSNR-SSIM-90% Quantile (Q.). We highlight the best number under each watermark and threshold. Note that TreeRing relies on thresholding the ℓ_1 distance for pattern matching, which is different from γ used in other watermarks. For fair comparison, we mask out cases where one evasion method cannot evade $\geq 90\%$ of the watermarked images.

Tree-Ring	Threshold	70	60	50	40
	TPR \uparrow / FPR \downarrow	1.00 / 0.01	1.00 / 0.00	0.99 / 0.00	0.95 / 0.00
Gaussian noise	PSNR - SSIM - Q.	**	16.49 - 0.19 - 70.6	23.06 - 0.42 - 32.9	25.75 - 0.53 - 22.3
JPEG		—	*28.45 - 0.78 - 17.2	31.37 - 0.86 - 12.3	34.64 - 0.92 - 8.4
bm3d		****	*26.40 - 0.79 - 14.6	28.66 - 0.85 - 10.2	29.47 - 0.88 - 8.5
DiffPure		23.20 - 0.63 - 31.8	27.79 - 0.77 - 18.7	29.79 - 0.83 - 14.1	30.16 - 0.84 - 13.0
Diffuser		—	****	**	*28.01 - 0.84 - 16.1
VAE		—	****	*34.06 - 0.89 - 9.0	*35.58 - 0.93 - 7.2
DIP (ours)		*12.28 - 0.42 - 102.7	17.67 - 0.59 - 64.4	26.14 - 0.79 - 26.1	34.11 - 0.93 - 9.6

The following markers are used for the purpose of fair comparison of the best evasion image quality:

— Evasion method only successfully evade $< 10\%$ of the watermarked images.

**** Evasion method only successfully evade $< 75\%$ of the watermarked images.

** Evasion method only successfully evade $< 90\%$ of the watermarked images.

* Evasion method successfully evade $\geq 90\%$ of the watermarked images, but $< 100\%$.

Experiment results As mentioned in Section 2, the choice of γ in the watermark decoder, as shown in Eq. (4), is highly task-dependent. It determines the true positive rate (TPR) and the false positive rate (FPR) in watermark detection—TPR measures the fraction of watermarked images correctly detected, and FPR measures the fraction of clean images wrongly flagged as watermarked images. In general, the higher the γ used in the decoder, the lower the true positive rate (TPR) and the false positive rate (FPR). A practically useful watermark decoder should have a TPR close to one and a FPR close to zero. On the other hand, the higher the γ , the higher the quality of the evasion image can achieve. To account for the effect of γ in robustness evaluation, we report in Table 2 the evasion performance of different methods under different γ 's on COCO images, and Table 3 on DiffusionDB images, together with the TPR/FPR achieved.

From Tables 2 to 4, we observe that: **(1)** The effect of γ on TPR/FPR values as well as image quality of different watermarks against the detection threshold agrees with our discussion above. This is true also for the TreeRing watermark, whose detection threshold is based on the ℓ_1 distance, very different from those for other watermark methods; **(2)** The performance of watermark evasion shown by the column with $\gamma = 0.55$ in Tables 2 and 3 is not quite meaningful—the very high FPR renders the decoder hardly useful in practice; **(3)** In other cases, there is no clear winner among all the evasion methods we evaluate. For example, our DIP-based evasion has the best performance on DwtDctSVD and rivaGAN, and is comparable to the best on SSL; DiffPure is the most effective evasion on TrustMark, RoSteALS and StegaStamp; TreeRing seems most vulnerable to JPEG compression. This highlights the need to include diverse sources of evasion methods for faithful robustness evaluation of watermarking systems, as we argue in Section 3.2.

Moreover, comparing the results of our DIP-based evasion on different watermarks, we observe that evasion images for DwtDctSVD, rivaGAN, and SSL watermarks can achieve very high quality when $\gamma \geq 0.65$, with reasonable TPR/FPR values. This is well expected, as these watermarks mainly cause high-frequency distortions (see Fig. 6), and DIP-based evasion is good at separating high- and low-frequency components and thereby largely removing the watermark during iteration, as argued in Section 3.2. In contrast, DIP-based evasion shows limited performance on RoSteALS and StegaStamp, as these watermark methods induce substantial mid- and low-frequency distortions, which DIP picks up in early stages so are hard to separate from the clean image content. DIP's mediocre performance on TrustMark is a bit surprising. One possible explanation is that TrustMark, in fact, induces mainly low-frequency distortions, which is downplayed in our visualization due to the log scale as shown in Fig. 6.

5 Conclusion and discussion

With the results and the analysis above, we can conclude that there is *no universal best evasion methods* for existing watermarking systems. In general, our DIP-based evasion is most effective in evading invisible watermarks that induce high-frequency distortions (e.g., DwtDctSVD, rivaGAN and SSL), and is partially successful in evading *in-processing* watermarks such as TreeRing. Its limited performance for RoSteALS and

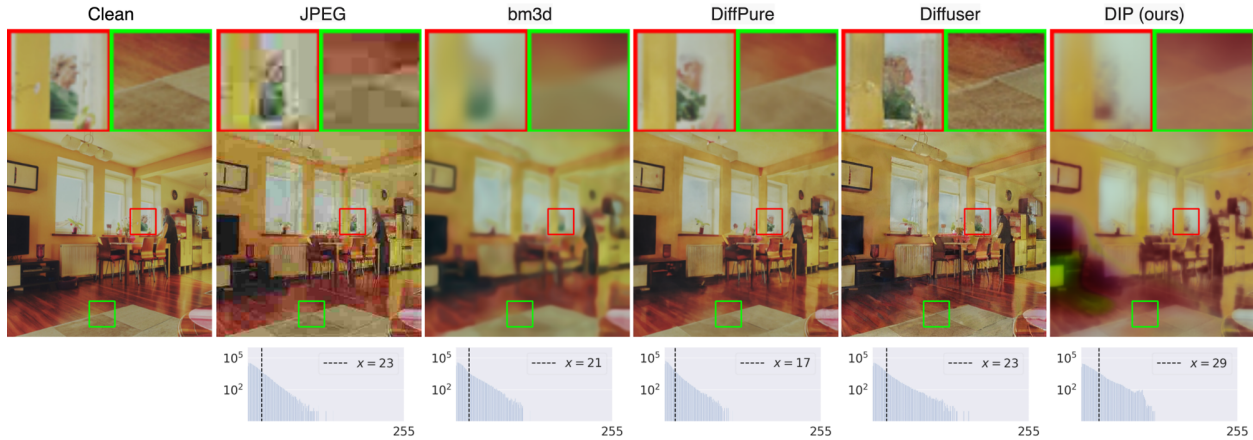


Figure 8: Visualization of the evasion images found by different evasion methods on a StegaStamp watermarked image (with $\gamma = 0.75$; top row) and the respective histograms of the pixel difference (y -axis in log scale) between the evasion image and the clean image (bottom row). The vertical dashed line marks the 90% quantile.

StegaStamp implies that exploiting low- and mid-frequency distortions is a viable way for watermarking systems to counteract our DIP-based evasion. Also, for these watermark methods, the regeneration evasion DiffPure has proved effective.

Moreover, for relatively visible watermarks (e.g., StegaStamp), the evasion images generated by all evasion methods always contain visible artifacts; see Fig. 8 for an example. Therefore, the future of learning-based watermarks is not all pessimistic: they may not be reliable for copyright protection, but may be promising in misinformation prevention. This is because of the distinct requirements of these two kinds of applications: for copyright protection, watermarks are expected to remain detectable as long as the image content is recognizable even under severe corruptions due to evasion—which may be too hard to achieve. In contrast, to prevent misinformation, it might be sufficient to achieve either of the following to mitigate the harm: **(i)** the watermark patterns can be detected by eyes, e.g., an overlaid logo or unnatural perturbations such as Figs. 1 and 8, raising suspicion that the image is already manipulated or fake; **(ii)** the watermark can be detected by an algorithmic decoder. For this purpose, watermarks such as StegaStamp may be sufficient.

Acknowledgments

Liang H. is partially supported by NIH fund R01NS131314. Sun J. is partially supported by NIH funds R01NS131314 and R01CA287413. The content is solely the responsibility of the authors and does not necessarily represent the official views of the National Institutes of Health. The authors acknowledge the Minnesota Supercomputing Institute (MSI) at the University of Minnesota for providing resources that contributed to the research results reported in this article.

References

- Bang An, Mucong Ding, Tahseen Rabbani, Aakriti Agrawal, Yuancheng Xu, Chenghao Deng, Sicheng Zhu, Abdirisak Mohamed, Yuxin Wen, Tom Goldstein, et al. Benchmarking the robustness of image watermarks. *arXiv preprint arXiv:2401.08573*, 2024.
- Diane Bartz and Krystal Hu. Openai, google, others pledge to watermark ai content for safety, white house says. <https://www.reuters.com/technology/openai-google-others-pledge-watermark-ai-content-safety-white-house-2023-07-21>.
- Ning Bi, Qiyu Sun, Daren Huang, Zhihua Yang, and Jiwu Huang. Robust image watermarking based on multiband wavelets and empirical mode decomposition. *IEEE Transactions on Image Processing*, 16(8): 1956–1966, 2007.

-
- Tu Bui, Shruti Agarwal, and John Collomosse. Trustmark: Universal watermarking for arbitrary resolution images. *arXiv preprint arXiv:2311.18297*, 2023a.
- Tu Bui, Shruti Agarwal, Ning Yu, and John Collomosse. Rosteals: Robust steganography using autoencoder latent space. In *Proceedings of the IEEE/CVF Conference on Computer Vision and Pattern Recognition*, pp. 933–942, 2023b.
- Zhengxue Cheng, Heming Sun, Masaru Takeuchi, and Jiro Katto. Learned image compression with discretized gaussian mixture likelihoods and attention modules. In *Proceedings of the IEEE/CVF conference on computer vision and pattern recognition*, pp. 7939–7948, 2020.
- Ingemar J Cox, Joe Kilian, F Thomson Leighton, and Talal Shamoon. Secure spread spectrum watermarking for multimedia. *IEEE transactions on image processing*, 6(12):1673–1687, 1997.
- Kostadin Dabov, Alessandro Foi, Vladimir Katkovnik, and Karen Egiazarian. Image denoising by sparse 3-d transform-domain collaborative filtering. *IEEE Transactions on image processing*, 16(8):2080–2095, 2007.
- Mingyuan Fan, Cen Chen, Chengyu Wang, and Jun Huang. On the trustworthiness landscape of state-of-the-art generative models: A comprehensive survey. *arXiv preprint arXiv:2307.16680*, 2023.
- Pierre Fernandez, Alexandre Sablayrolles, Teddy Furon, Hervé Jégou, and Matthijs Douze. Watermarking images in self-supervised latent spaces. In *ICASSP 2022-2022 IEEE International Conference on Acoustics, Speech and Signal Processing (ICASSP)*, pp. 3054–3058. IEEE, 2022.
- Pierre Fernandez, Guillaume Couairon, Hervé Jégou, Matthijs Douze, and Teddy Furon. The stable signature: Rooting watermarks in latent diffusion models. In *Proceedings of the IEEE/CVF International Conference on Computer Vision*, pp. 22466–22477, 2023.
- Ian Goodfellow, Jean Pouget-Abadie, Mehdi Mirza, Bing Xu, David Warde-Farley, Sherjil Ozair, Aaron Courville, and Yoshua Bengio. Generative adversarial nets. *Advances in neural information processing systems*, 27, 2014a.
- Ian J Goodfellow, Jonathon Shlens, and Christian Szegedy. Explaining and harnessing adversarial examples. *arXiv preprint arXiv:1412.6572*, 2014b.
- Sam Gunn, Xuandong Zhao, and Dawn Song. An undetectable watermark for generative image models. *IACR Cryptol. ePrint Arch.*, 2024:1597, 2024. URL <https://api.semanticscholar.org/CorpusID:273202887>.
- Alain Hore and Djemel Ziou. Image quality metrics: Psnr vs. ssim. In *2010 20th international conference on pattern recognition*, pp. 2366–2369. IEEE, 2010.
- Ming-Shing Hsieh, Din-Chang Tseng, and Yong-Huai Huang. Hiding digital watermarks using multiresolution wavelet transform. *IEEE Transactions on industrial electronics*, 48(5):875–882, 2001.
- Zhaoyang Jia, Han Fang, and Weiming Zhang. Mbrs: Enhancing robustness of dnn-based watermarking by mini-batch of real and simulated jpeg compression. In *Proceedings of the 29th ACM international conference on multimedia*, pp. 41–49, 2021.
- Zhengyuan Jiang, Jinghuai Zhang, and Neil Zhenqiang Gong. Evading watermark based detection of ai-generated content. In *Proceedings of the 2023 ACM SIGSAC Conference on Computer and Communications Security*, pp. 1168–1181, 2023.
- Yeonsik Jo, Se Young Chun, and Jonghyun Choi. Rethinking deep image prior for denoising. In *2021 IEEE/CVF International Conference on Computer Vision, ICCV 2021, Montreal, QC, Canada, October 10-17, 2021*, pp. 5067–5076. IEEE, 2021. doi: 10.1109/ICCV48922.2021.00504. URL <https://doi.org/10.1109/ICCV48922.2021.00504>.
- Mohan S Kankanhalli, KR Ramakrishnan, et al. Adaptive visible watermarking of images. In *Proceedings IEEE International Conference on Multimedia Computing and Systems*, volume 1, pp. 568–573. IEEE, 1999.

-
- Diederik P Kingma and Jimmy Ba. Adam: A method for stochastic optimization. *arXiv preprint arXiv:1412.6980*, 2014.
- Taihui Li, Zhong Zhuang, Hengyue Liang, Le Peng, Hengkang Wang, and Ju Sun. Self-validation: Early stopping for single-instance deep generative priors. *arXiv preprint arXiv:2110.12271*, 2021.
- Taihui Li, Hengkang Wang, Zhong Zhuang, and Ju Sun. Deep random projector: Accelerated deep image prior. In *Proceedings of the IEEE/CVF Conference on Computer Vision and Pattern Recognition*, pp. 18176–18185, 2023a.
- Taihui Li, Zhong Zhuang, Hengkang Wang, and Ju Sun. Random Projector: Efficient Deep Image Prior. In *ICASSP 2023 - 2023 IEEE International Conference on Acoustics, Speech and Signal Processing (ICASSP)*, pp. 1–5, June 2023b. doi: 10.1109/ICASSP49357.2023.10097088.
- Taihui Li, Anish Lahiri, Yutong Dai, and Owen Mayer. Joint demosaicing and denoising with double deep image priors. In *ICASSP 2024 - 2024 IEEE International Conference on Acoustics, Speech and Signal Processing (ICASSP)*, pp. 4005–4009, 2024. doi: 10.1109/ICASSP48485.2024.10448384.
- Tsung-Yi Lin, Michael Maire, Serge Belongie, James Hays, Pietro Perona, Deva Ramanan, Piotr Dollár, and C Lawrence Zitnick. Microsoft coco: Common objects in context. In *Computer Vision—ECCV 2014: 13th European Conference, Zurich, Switzerland, September 6–12, 2014, Proceedings, Part V 13*, pp. 740–755. Springer, 2014.
- Xiyang Luo, Ruohan Zhan, Huiwen Chang, Feng Yang, and Peyman Milanfar. Distortion agnostic deep watermarking. In *Proceedings of the IEEE/CVF conference on computer vision and pattern recognition*, pp. 13548–13557, 2020.
- Gary Mataev, Peyman Milanfar, and Michael Elad. Deepred: Deep image prior powered by red. In *Proceedings of the IEEE/CVF International Conference on Computer Vision Workshops*, pp. 0–0, 2019.
- Jennifer Mishra. How to remove dall-e watermark, 2022. URL <https://www.youtube.com/watch?v=6EMROCxGCIA>.
- Tayana Morkel, Jan HP Eloff, and Martin S Olivier. An overview of image steganography. In *ISSA*, volume 1, pp. 1–11, 2005.
- Alhassan Mumuni and Fuseini Mumuni. Data augmentation: A comprehensive survey of modern approaches. *Array*, 16:100258, 2022.
- KA Navas, Mathews Cheriyan Ajay, M Lekshmi, Tampy S Archana, and M Sasikumar. Dwt-dct-svd based watermarking. In *2008 3rd international conference on communication systems software and middleware and workshops (COMSWARE'08)*, pp. 271–274. IEEE, 2008.
- Shelby Pereira and Thierry Pun. Fast robust template matching for affine resistant image watermarks. In *International Workshop on Information Hiding*, pp. 199–210. Springer, 1999.
- Shelby Pereira and Thierry Pun. Robust template matching for affine resistant image watermarks. *IEEE transactions on image Processing*, 9(6):1123–1129, 2000.
- Adnan Qayyum, Inaam Ilahi, Fahad Shamshad, Farid Boussaïd, Mohammed Bennamoun, and Junaid Qadir. Untrained neural network priors for inverse imaging problems: A survey. *IEEE Trans. Pattern Anal. Mach. Intell.*, 45(5):6511–6536, 2023. doi: 10.1109/TPAMI.2022.3204527. URL <https://doi.org/10.1109/TPAMI.2022.3204527>.
- Aditya Ramesh, Prafulla Dhariwal, Alex Nichol, Casey Chu, and Mark Chen. Hierarchical text-conditional image generation with clip latents. *arXiv preprint arXiv:2204.06125*, 1(2):3, 2022.
- Mouryam Rishik. Watermark removal using deep image priors with pytorch. <https://github.com/braindotai/Watermark-Removal-Pytorch/commits/master>.

-
- Robin Rombach, Andreas Blattmann, Dominik Lorenz, Patrick Esser, and Björn Ommer. High-resolution image synthesis with latent diffusion models. In *Proceedings of the IEEE/CVF conference on computer vision and pattern recognition*, pp. 10684–10695, 2022.
- Mehrdad Saberi, Vinu Sankar Sadasivan, Keivan Rezaei, Aounon Kumar, Atoosa Chegini, Wenxiao Wang, and Soheil Feizi. Robustness of ai-image detectors: Fundamental limits and practical attacks. *arXiv preprint arXiv:2310.00076*, 2023.
- Gustavo Santana. Stable diffusion dataset. <https://huggingface.co/datasets/Gustavosta/Stable-Diffusion-Prompts>. Accessed: 2025-02-16.
- Zenglin Shi, Pascal Mettes, Subhransu Maji, and Cees G. M. Snoek. On measuring and controlling the spectral bias of the deep image prior. *Int. J. Comput. Vis.*, 130(4):885–908, 2022a. doi: 10.1007/S11263-021-01572-7. URL <https://doi.org/10.1007/s11263-021-01572-7>.
- Zenglin Shi, Pascal Mettes, Subhransu Maji, and Cees GM Snoek. On measuring and controlling the spectral bias of the deep image prior. *International Journal of Computer Vision*, 130(4):885–908, 2022b.
- Matthew Tancik, Ben Mildenhall, and Ren Ng. Stegastamp: Invisible hyperlinks in physical photographs. In *Proceedings of the IEEE/CVF conference on computer vision and pattern recognition*, pp. 2117–2126, 2020.
- Tom Tirer, Raja Giryes Se, Young Chun, Yonina C. Eldar, ©SHUTTERSTOCK.COM, and Andrew Krasovitchii. Deep internal learning: Deep learning from a single input. *IEEE Signal Processing Magazine*, 41: 40–57, 2023. URL <https://api.semanticscholar.org/CorpusID:266174018>.
- Anatol Z Tirkel, GA Rankin, RM Van Schyndel, WJ Ho, NRA Mee, and Charles F Osborne. Electronic watermark. *Digital Image Computing, Technology and Applications (DICTA '93)*, pp. 666–673, 1993.
- Dmitry Ulyanov, Andrea Vedaldi, and Victor Lempitsky. Deep image prior. In *Proceedings of the IEEE conference on computer vision and pattern recognition*, pp. 9446–9454, 2018.
- George Voyatzis and Ioannis Pitas. Protecting digital image copyrights: a framework. *IEEE Computer Graphics and Applications*, 19(1):18–24, 1999.
- Hengkang Wang, Taihui Li, Zhong Zhuang, Tiancong Chen, Hengyue Liang, and Ju Sun. Early stopping for deep image prior. *arXiv preprint arXiv:2112.06074*, 2021.
- Hengkang Wang, Xu Zhang, Taihui Li, Yuxiang Wan, Tiancong Chen, and Ju Sun. Dmplug: A plug-in method for solving inverse problems with diffusion models. *arXiv preprint arXiv:2405.16749*, 2024.
- Zijie J Wang, Evan Montoya, David Munechika, Haoyang Yang, Benjamin Hoover, and Duen Horng Chau. Diffusiondb: A large-scale prompt gallery dataset for text-to-image generative models. *arXiv preprint arXiv:2210.14896*, 2022.
- Bingyang Wen and Sergul Aydore. Romark: A robust watermarking system using adversarial training. *arXiv preprint arXiv:1910.01221*, 2019.
- Yuxin Wen, John Kirchenbauer, Jonas Geiping, and Tom Goldstein. Tree-ring watermarks: Fingerprints for diffusion images that are invisible and robust. *arXiv preprint arXiv:2305.20030*, 2023.
- Mike Wendling. Ai can be easily used to make fake election photos - report. <https://www.bbc.com/news/world-us-canada-68471253>.
- Zijin Yang, Kai Zeng, Kejiang Chen, Han Fang, Wei Ming Zhang, and Neng H. Yu. Gaussian shading: Provable performance-lossless image watermarking for diffusion models. *2024 IEEE/CVF Conference on Computer Vision and Pattern Recognition (CVPR)*, pp. 12162–12171, 2024. URL <https://api.semanticscholar.org/CorpusID:269004589>.
- Ning Yu, Vladislav Skripniuk, Sahar Abdelnabi, and Mario Fritz. Artificial fingerprinting for generative models: Rooting deepfake attribution in training data. In *Proceedings of the IEEE/CVF International conference on computer vision*, pp. 14448–14457, 2021.

Kevin Alex Zhang, Alfredo Cuesta-Infante, Lei Xu, and Kalyan Veeramachaneni. Steganogan: High capacity image steganography with gans. *arXiv preprint arXiv:1901.03892*, 2019a.

Kevin Alex Zhang, Lei Xu, Alfredo Cuesta-Infante, and Kalyan Veeramachaneni. Robust invisible video watermarking with attention. *arXiv preprint arXiv:1909.01285*, 2019b.

Richard Zhang, Phillip Isola, Alexei A Efros, Eli Shechtman, and Oliver Wang. The unreasonable effectiveness of deep features as a perceptual metric. In *Proceedings of the IEEE conference on computer vision and pattern recognition*, pp. 586–595, 2018.

Xuandong Zhao, Kexun Zhang, Zihao Su, Saastha Vasana, Ilya Grishchenko, C Kruegel, G Vigna, YX Wang, and L Li. Invisible image watermarks are provably removable using generative ai. *Saastha Vasana, Ilya Grishchenko, Christopher Kruegel, Giovanni Vigna, Yu-Xiang Wang, and Lei Li, “Invisible image watermarks are provably removable using generative ai,” Aug, 2023.*

Xuandong Zhao, Sam Gunn, Miranda Christ, Jaiden Fairuze, Andres Fabrega, Nicholas Carlini, Sanjam Garg, Sanghyun Hong, Milad Nasr, Florian Tramèr, Somesh Jha, Lei Li, Yu-Xiang Wang, and Dawn Song. Sok: Watermarking for ai-generated content. *ArXiv*, abs/2411.18479, 2024. URL <https://api.semanticscholar.org/CorpusID:274305578>.

Jiren Zhu, Russell Kaplan, Justin Johnson, and Li Fei-Fei. Hidden: Hiding data with deep networks. In *Proceedings of the European conference on computer vision (ECCV)*, pp. 657–672, 2018.

Zhong Zhuang. *Advancing Deep Learning for Scientific Inverse Problems*. PhD thesis, University of Minnesota, 2023.

Zhong Zhuang, David Yang, Felix Hofmann, David Barmherzig, Ju Sun, David Yang, Felix Hofmann, David Barmherzig, and Ju Sun. Practical phase retrieval using double deep image priors. *Electronic Imaging*, 35:1–6, January 2023. ISSN 2470-1173. doi: 10.2352/EI.2023.35.14.COIMG-153. URL <https://library.imaging.org/ei/articles/35/14/COIMG-153>. Publisher: Society for Imaging Science and Technology.

Zhong Zhuang, Taihui Li, Hengkang Wang, and Ju Sun. Blind image deblurring with unknown kernel size and substantial noise. *International Journal of Computer Vision*, 132(2):319–348, 2024.

A DALLE-2 visible watermark

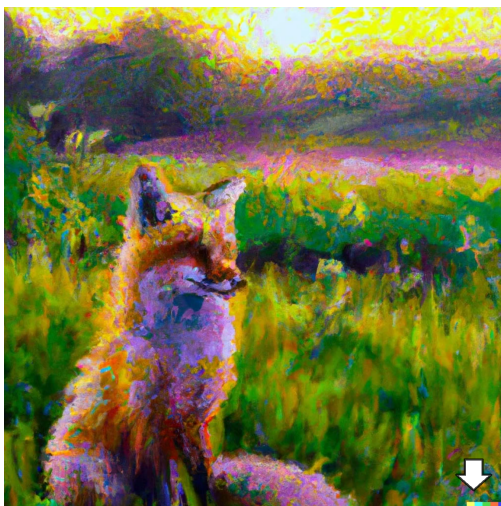


Figure 9: An example image generated by DALLE-2 from the official website: <https://openai.com/index/dall-e-2/>, where the color code watermark is visible at the bottom-right corner.

Table 5: Details of hyperparameters used in our exhaustive search

Evasion method	Hyperparameter	Search range	Search resolution	Common default value
brightness	Enhancement factor	[0.01, 1]	0.01	0.5
contrast	Enhancement factor	[0.01, 1]	0.01	0.5
Gaussian Noise	Standard deviation	[0.01, 1]	0.01	0.1
JPEG	Quality factor	[1, 100]	1	50
bm3d	Noise standard deviation	[0.1, 5]	0.05	0.1
DiffPure	Diffusion noise level	[0.1, 1]	0.1	0.1 - 0.3
Diffuser	Diffusion inverse steps	[10, 100]	10	60
VAE-Cheng2020	VAE compression quality index	[1, 6]	1	3
DIP (ours)	Number of iteration	[1, 500]	10	-

B Ranges of hyperparameters of various evasion methods

Table 5 presents the range of each hyperparameter and the grid resolution in our exhaustive search. If we simply use these typical values without exhaustive search, it is very likely that we will overestimate the level of robustness and underestimate the evasion image quality. Fig. 10 shows an example of the exhaustive search process on our DIP-based evasion.

In Table 5, the quality index of VAE indexes the individual pretrained model (six provided in the original work). Thus, the minimal resolution for VAE search is 1 and cannot be smaller. Moreover, the last column shows the typical value used in the existing literature for robustness evaluation as a reference, e.g., Zhao et al. (2023); Saberi et al. (2023). To the best of our knowledge, the reason why these values are chosen as defaults is not well justified.

C Image quality v.s. evasion success

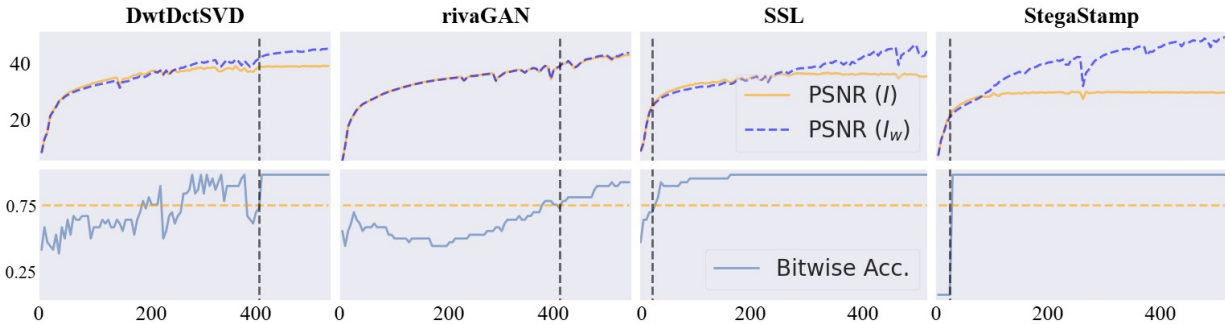


Figure 10: The PSNR trajectories of DIP-based evasion (top row) with respect to the watermarked image (in blue) and with respect to the original image (orange), and the corresponding trajectory of evasion performance (bottom row, measured by BA), for different watermark systems. Consider the BA threshold $\gamma = 0.75$ for detection (marked by horizontal orange lines). The vertical black lines mark the best-quality evasion images.

D Additional visualization of evasion image quality on rivaGAN

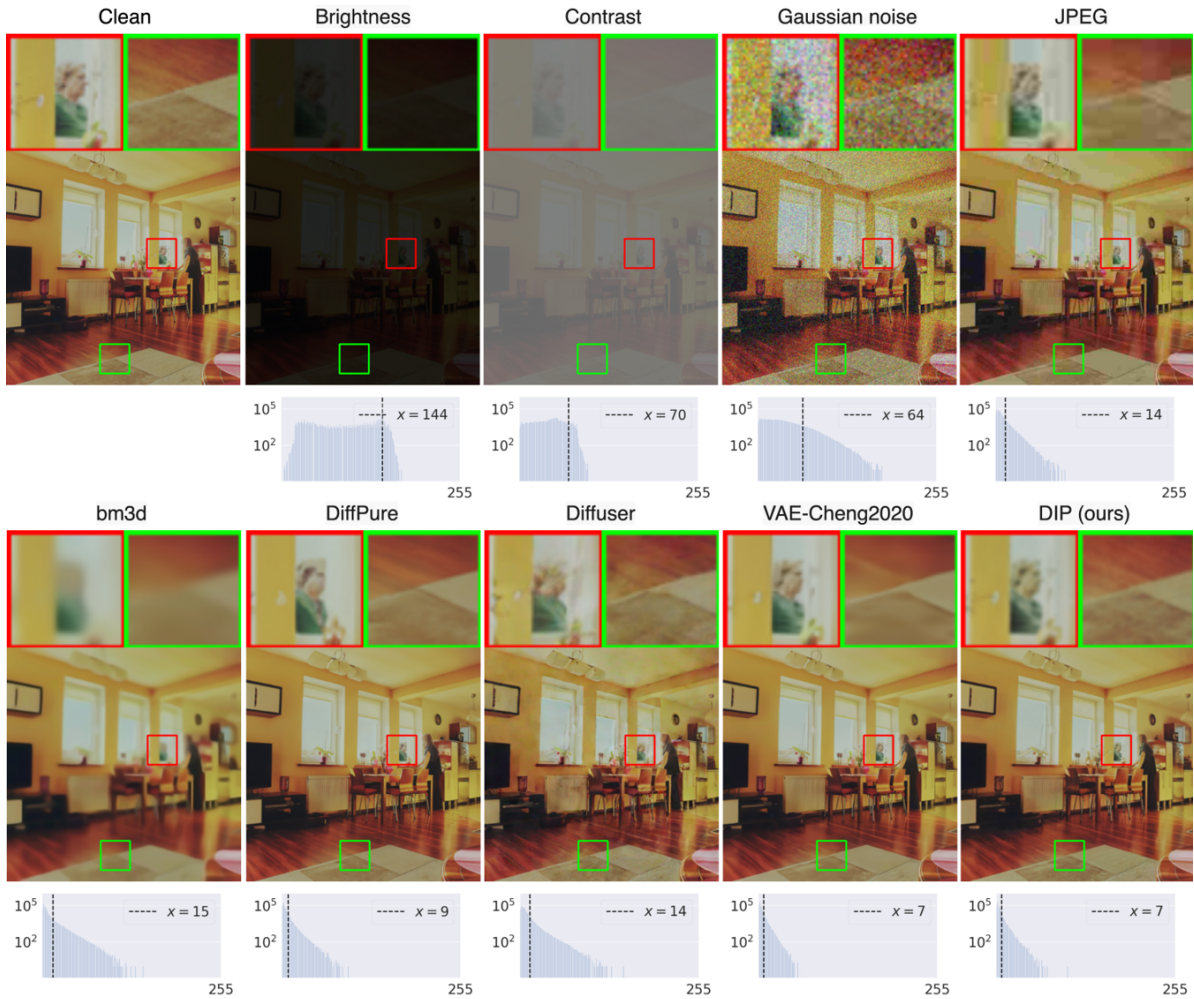


Figure 11: Visualization of the evasion images found by different evasion methods on a rivaGAN watermarked image (with $\gamma = 0.75$; top row) and the respective histograms of the pixel difference (y -axis in log scale) between the evasion image and the clean image (bottom row). The vertical dashed line marks the 90% quantile. We can observe that the evasion image produced by DIP has almost no loss of image quality.